a)

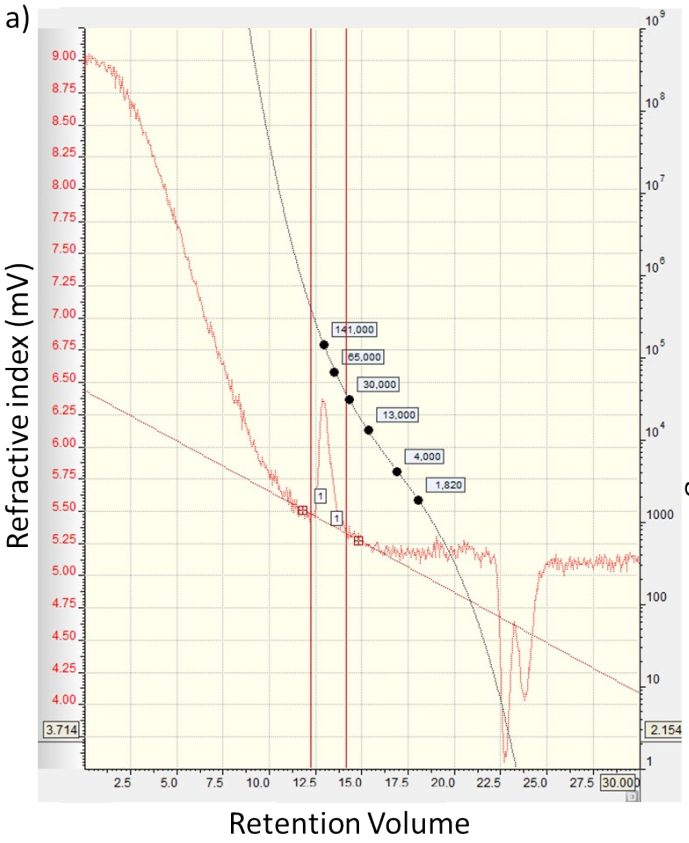

b)

From GPC Calculations	
Peak	1
Retention Volume (mL)	12.997
Mn (Da)	150,204
Mw (Da)	217,602
Mz (Da)	253,905
Mp (Da)	137,342
Mw/Mn	1.358
From Aldrich SDS	
Styrene Weight Percent (%)	22

c)

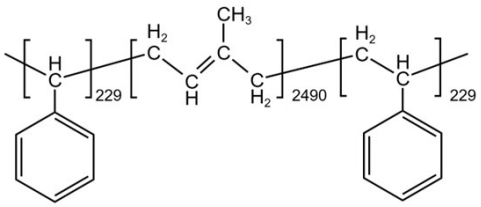

Polystyrene-*block*-polyisoprene-*block*-polystyrene

Figure S1: a) readout from Gel Permeation Chromatography for Polystyrene-block-Polyisoprene-block-Polystyrene (PS-PI-PS) purchased from Aldrich Chemistry. b) calculated parameters for the PS-PI-PS from the GPC data c) polymer structure with specific block lengths

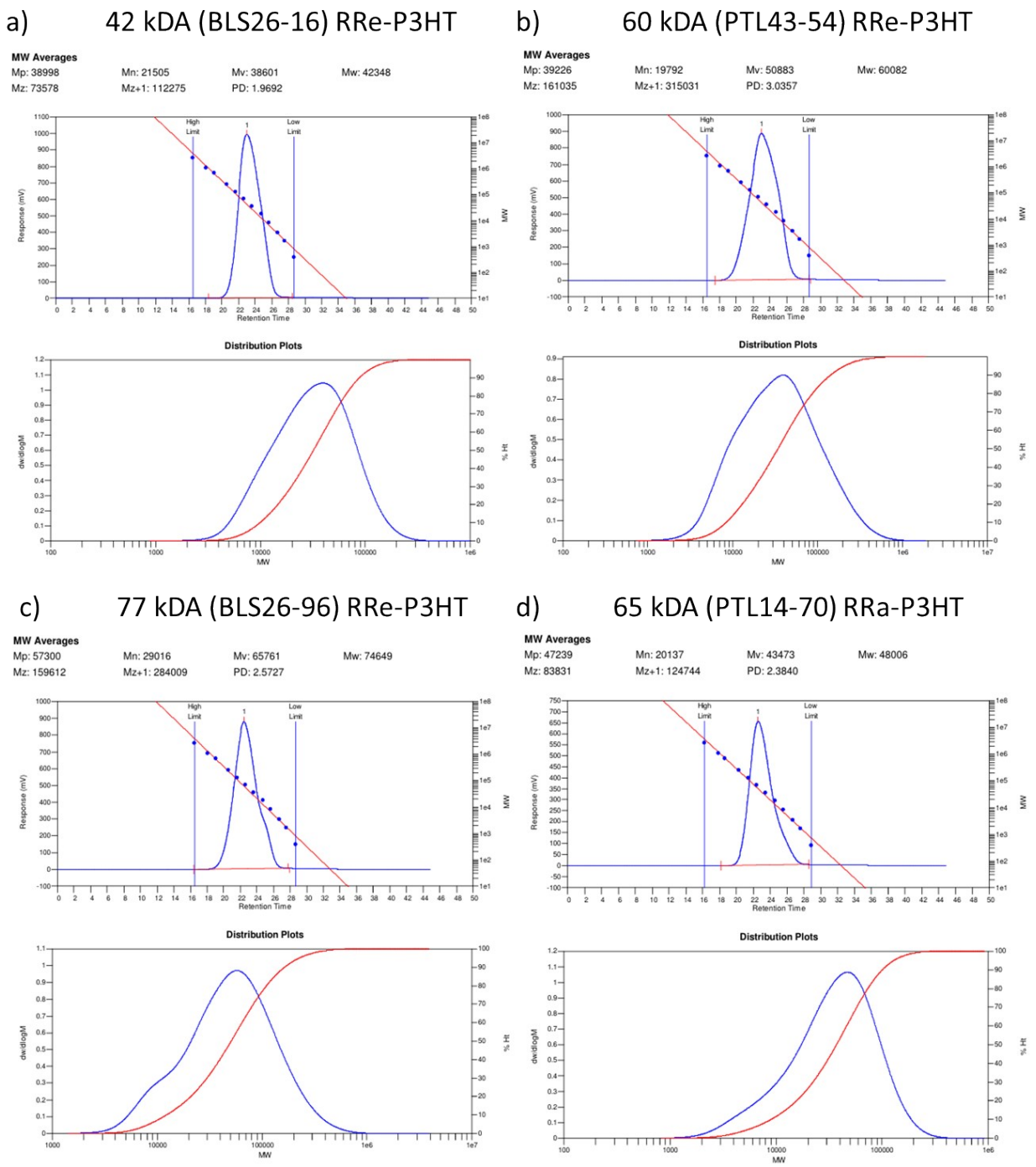

Figure S2: GPC data provided by Rieke metals for the RRe-P3HT of all molecular weights – 42 kDA (a), 60 kDa (b), 77 kDa (c) – and RRa-P3HT (d) used in this work.

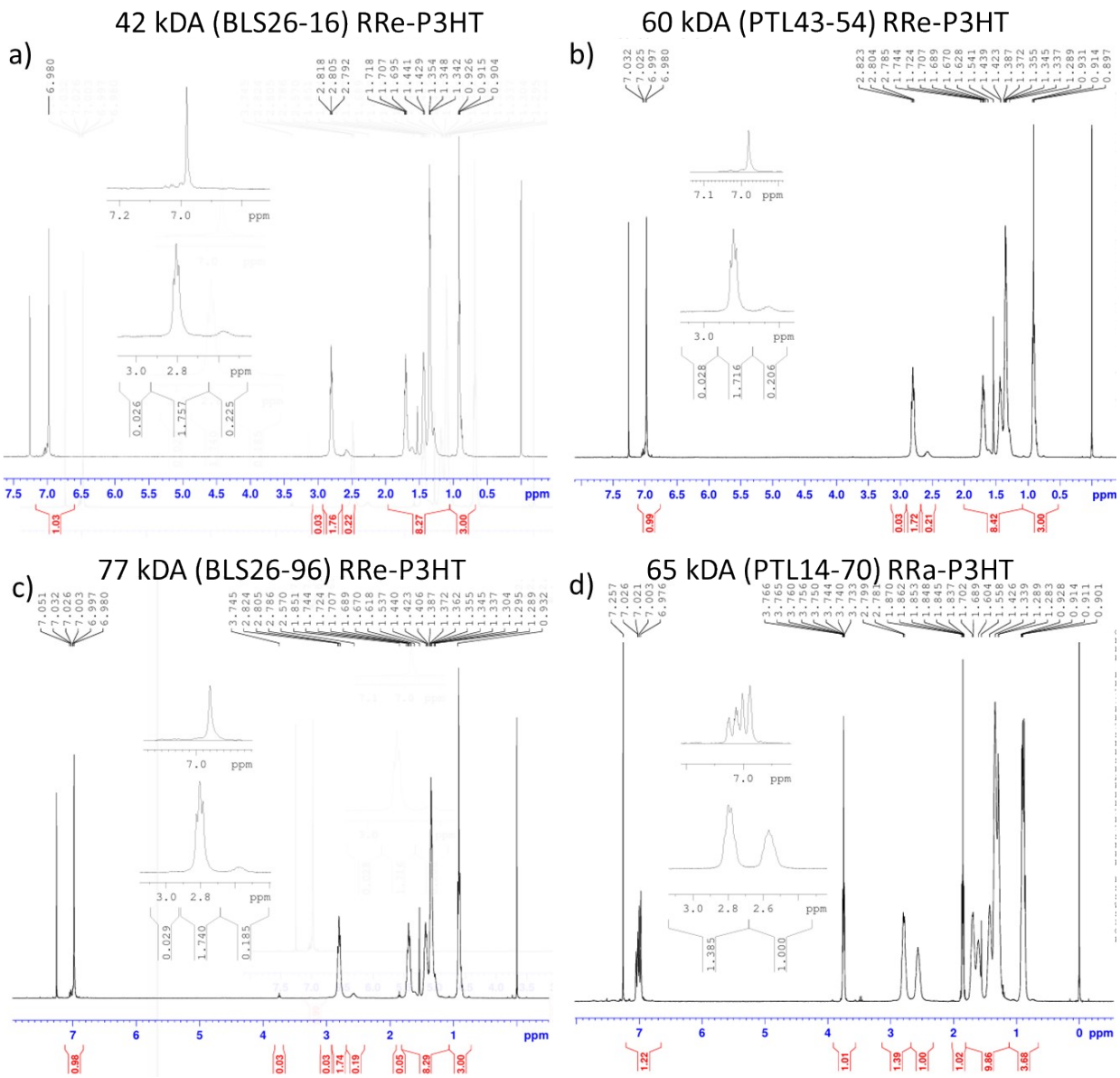

Figure S3: NMR data provided by Rieke metals for the RRe-P3HT of all molecular weights – 42 kDA (a), 60 kDa (b), 77 kDa (c) – and RRa-P3HT (d) used in this work

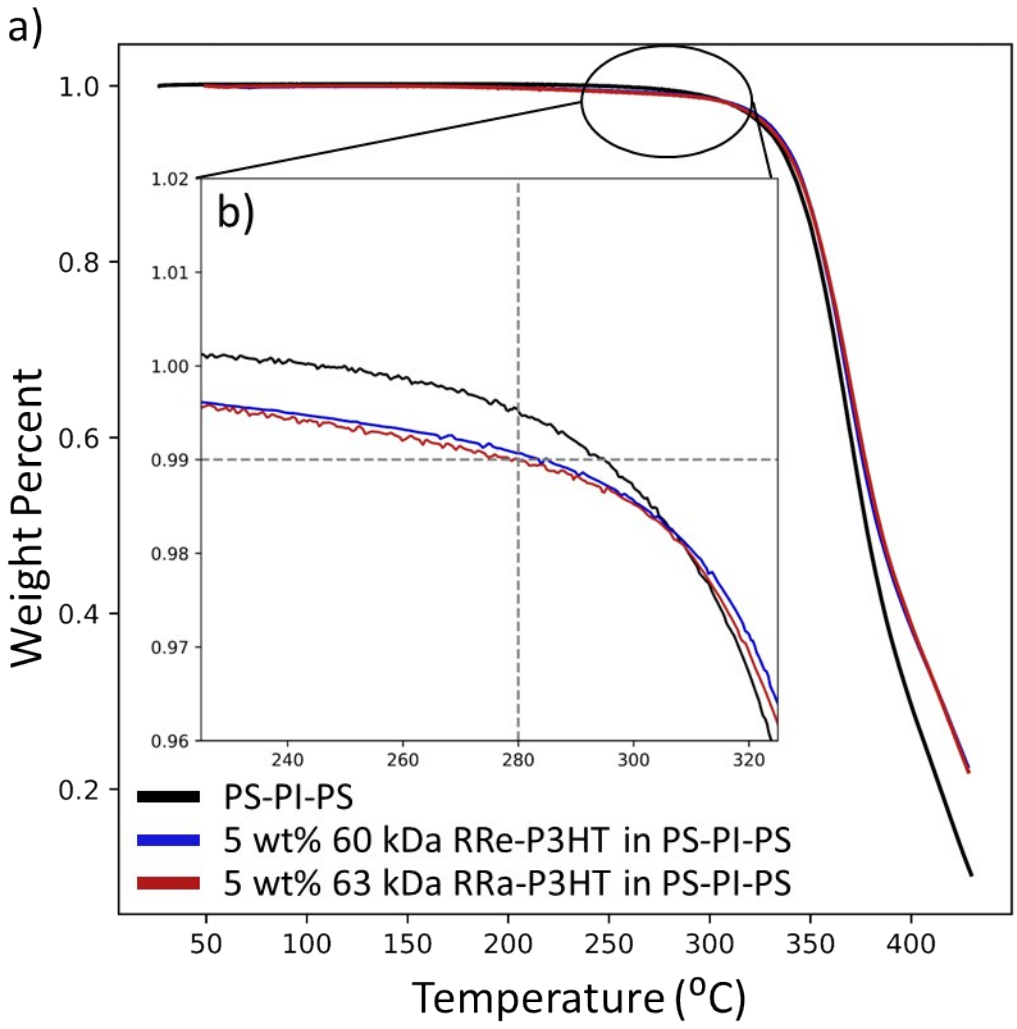

Figure S4: a) thermogravimetric analysis (TGA) of pure PS-PI-PS matrix, a blend of 5 wt% RRa-P3HT in 95 wt% PS-PI-PS, and a blend of 5 wt% RRe-P3HT in 95 wt% PS-PI-PS for full temperature scale (heated at 10 ºC/minute between 23 ºC to 400 ºC) b) zoomed in region of interest with guidelines to denote where the material has lost 1% of its total mass

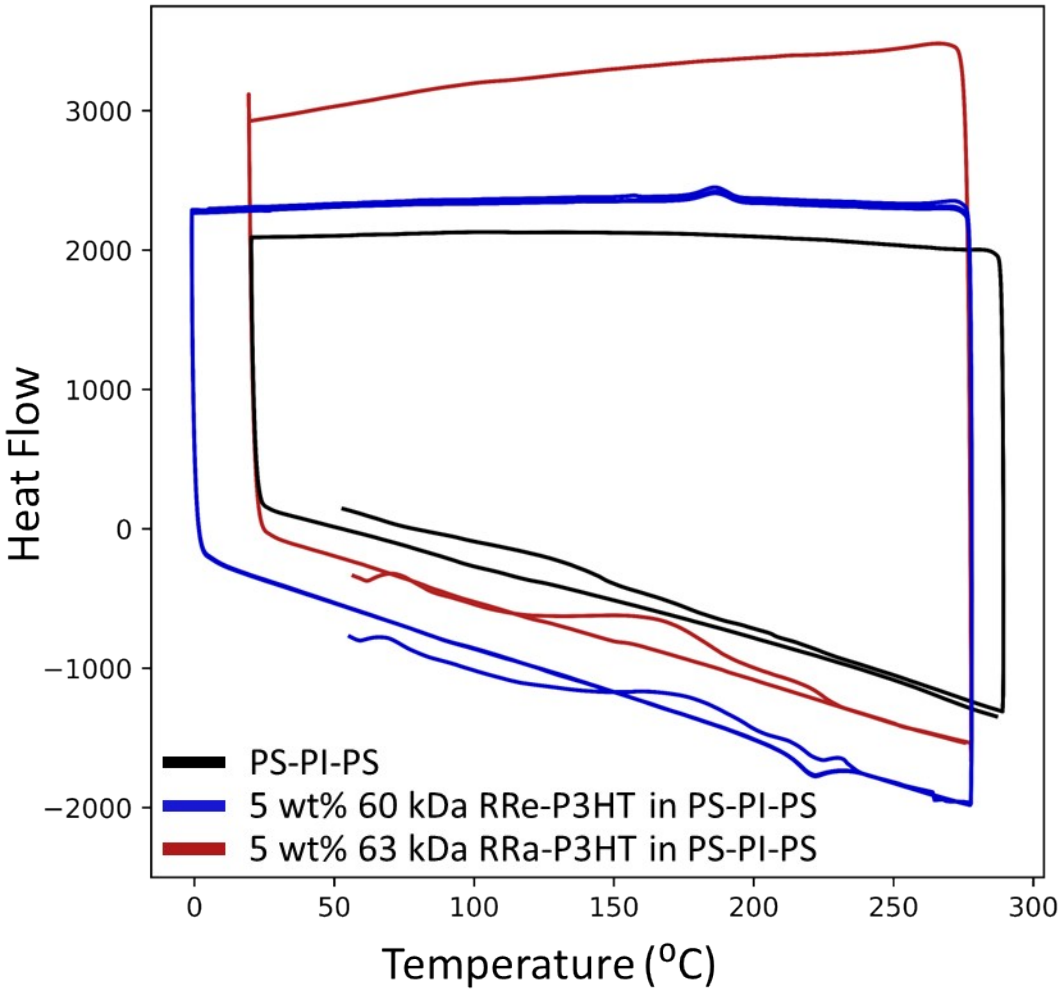

Figure S5: Full temperature range for Differential Scanning Calorimetry (DSC) measurements conducted between 0 ºC and 280 ºC for 5 wt% RRe-P3HT in PS-PI-PS and 23 ºC and 280 ºC for 5 wt% RRa-P3HT in PS-PI-PS and pure PS-PI-PS. The RRe-P3HT in PS-PI-PS and the PS-PI-PS were run for three heating cycles (heat-cool-heat-cool-heat-cool) while the RRa-P3HT in PS-PI-PS was run for two heating cycles (heat-cool-heat) and all cycles are shown. Multiple heating cycles were run to remove thermal history, and the second heat is shown in **Figure 1f**. Multiple heating cycles were run to remove thermal history, and the second heating sequence is shown in Figure 1f. Heating was conducted at a rate of 10 ºC/min and cooling was done at 5 ºC/min for all samples.

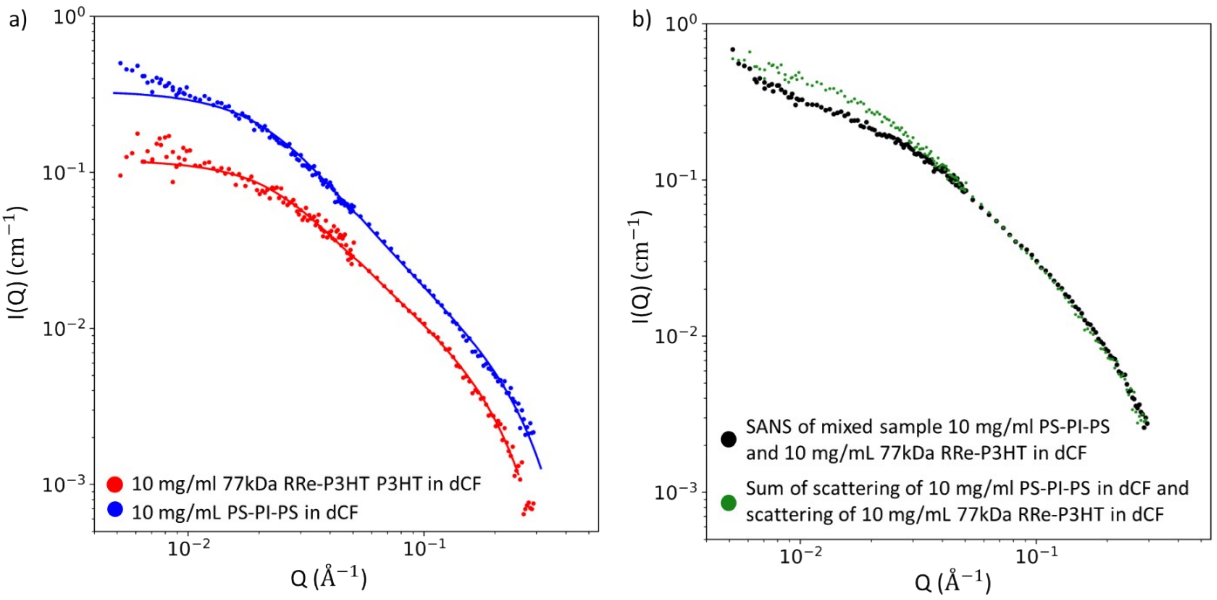

Figure S6: SANS plots of a) free polymer chains of 10 mg/ mL PS-PI-PS in chloroform-d and 10 mg/mL 77 kDa RRe-P3HT in chloroform-d. The data is fit with models of flexible cylinders which are shown with solid lines. b) SANS plot of experimentally run mixed sample of (black data points) 10 mg/mL PS-PI-PS and 10 mg/mL of 77kDa RRe-P3HT in chloroform-d and (green data points) data of the arithmetic sum of the scattering of the individual components: 10 mg/mL 77kDa RRe-P3HT in dCF (red data in Figure 3a) and 10 mg/mL PS-PI-PS in dCF (blue data in Figure 3a).

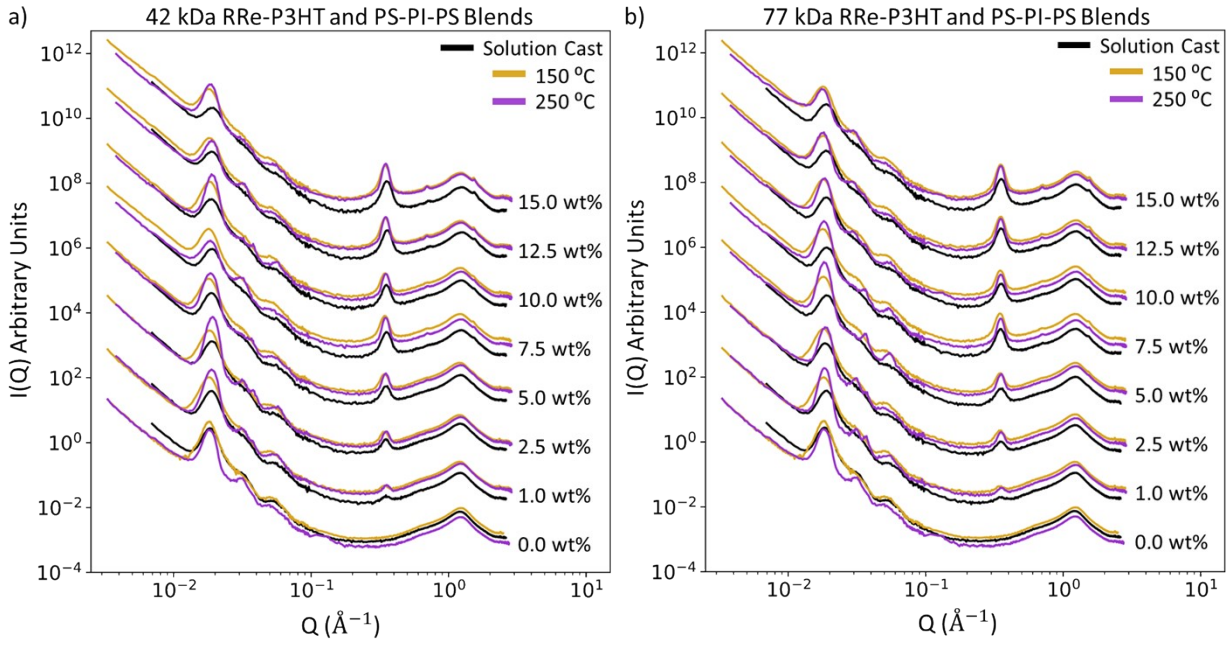

Figure S7: a) SAXS data of 42 kDA RRe-P3HT and PS-PI-PS blends, labeled by wt% of RRe-P3HT added to system, and collected after solution casting and two different heat pressing temperatures. Data is arbitrarily shifted to separate samples into wt%s. b) SAXS data of 77 kDA RRe-P3HT and PS-PI-PS blends, labeled by wt% of RRe-P3HT added to system, and collected after solution casting and two different heat pressing temperatures. Data is arbitrarily shifted to separate samples into wt%s.

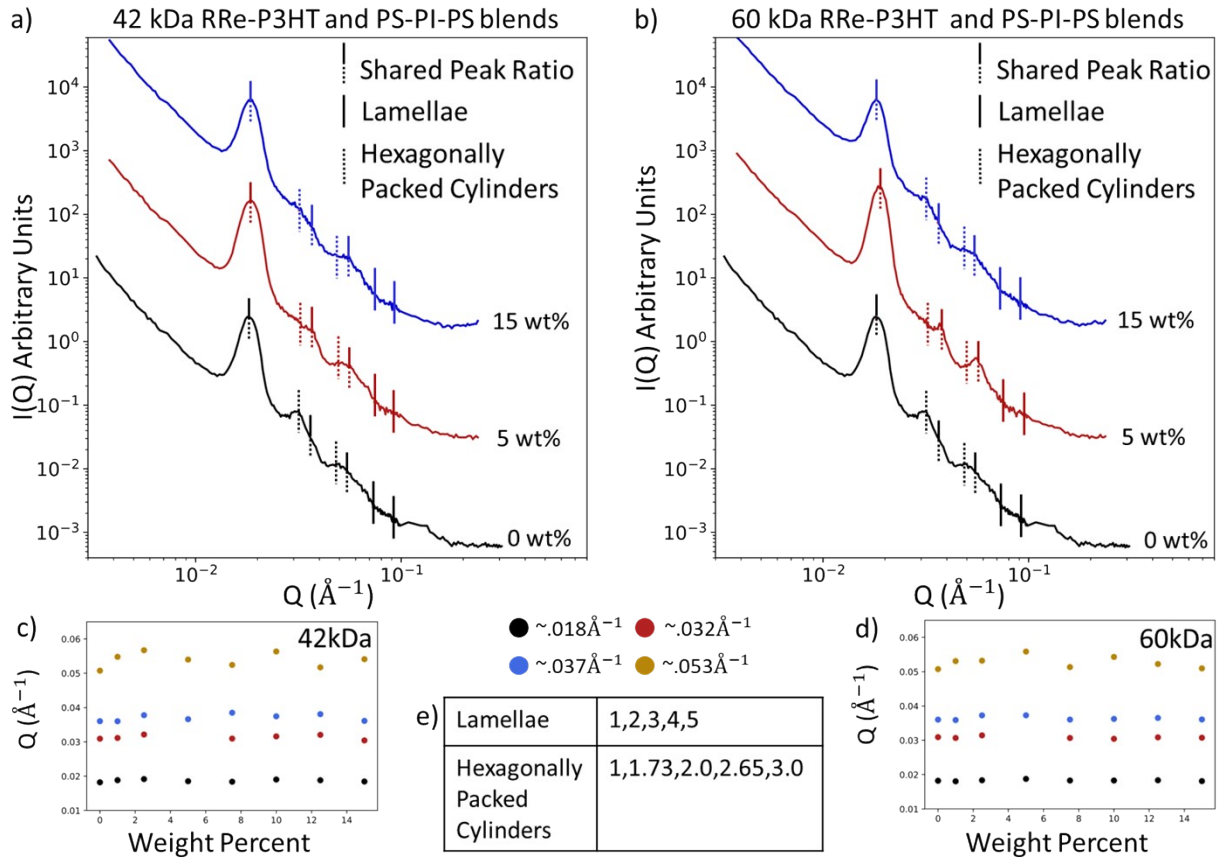

Figure S8: a) SAXS data of selected 42 kDA RRe-P3HT and PS-PI-PS blends, labeled by wt% of RRe-P3HT added to system, and collected at 250 ºC. Data is arbitrarily shifted to separate samples into wt%. Lines are added to mark where peaks are expected for lamellar and hexagonally packed cylinder structures. Some locations overlap between the two and are noted with solid lines. b) SAXS data of selected 60 kDA RRe-P3HT and PS-PI-PS blends, labeled by wt% of RRe-P3HT added to system, and collected at 250 ºC. Data is arbitrarily shifted to separate samples into wt%. Lines are added to mark where peaks are expected for lamellar and hexagonally packed cylinder structures. Some locations overlap between the two and are noted with solid lines.c) 42 kDA RRe-

P3HT and PS-PI-PS blends peak position parameters from broad peak fits of all peaks with colors dictated by legend above. d) 60 kDA RRe-P3HT and PS-PI-PS blends peak position parameters from broad peak fits of all peaks with colors dictated by legend above. e) known ratios for lamellar and hexagonally packed cylinder phases

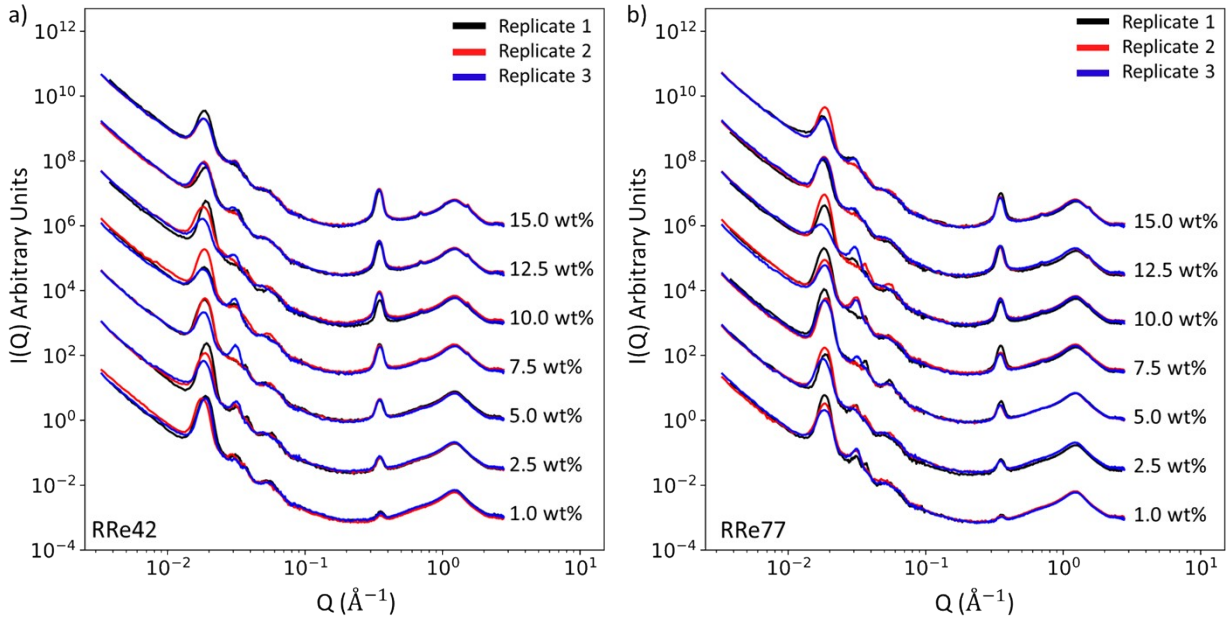

Figure S9: a) replicates of blends of 42 kDa RRe-P3HT and PS-PI-PS blends processed at 250 ºC b) replicates of blends of 77 kDa RRe-P3HT and PS-PI-PS blends processed at 250 ºC, note the morphological variation in compositionally identical samples in the 2.5 wt% to 10 wt% range. A zoomed in focus on the peak range of interest is provided in **Figure S10c** and **Figure S10d**.

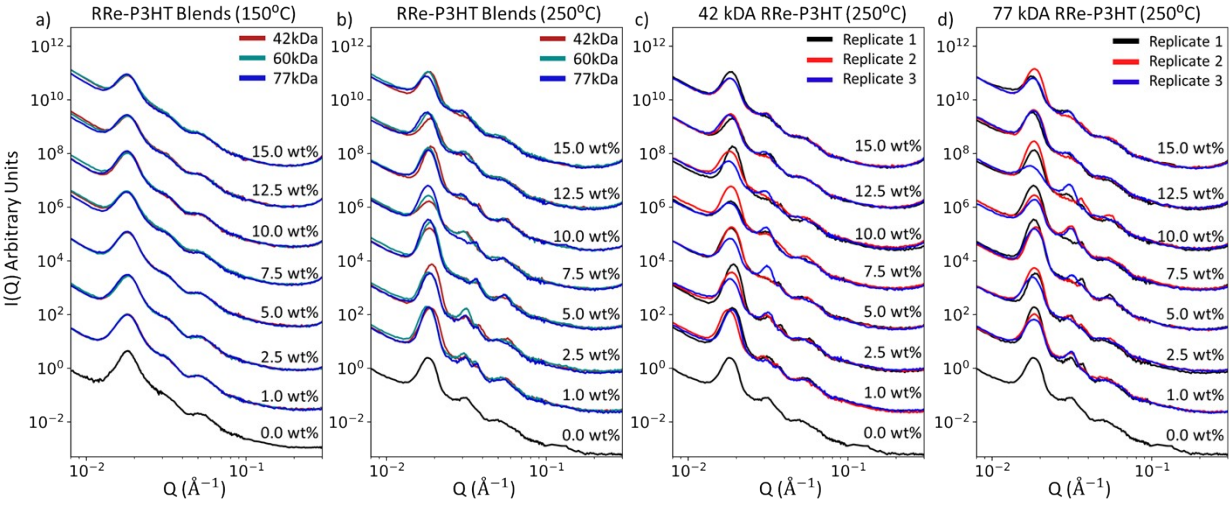

Figure S10: Zoomed in focus on the peaks of interest for a) **Figure 7a**, RRe-P3HT films of various molecular weights at 150 ºC, b) **Figure 8a**, RRe-P3HT films of various molecular weights at 250 ºC, c) **Figure S9a**, replicates of the 44 kDA RRe-P3HT processed at 250 ºC and d) **Figure S9b**, replicates of 77 kDA RRe-P3HT films of processed at 250 ºC

Sample Information		**Peak Ratios** $(\frac{Q_{peak\ i}}{Q_{peak\ 1}})$				**Phase**
Molecular Weight of RRe-P3HT	*Wt % of RRe-P3HT*	*Peak 1 (~.018Å^{-1})*	*Peak 2 (~.032Å^{-1})*	*Peak 3 (~.037Å^{-1})*	*Peak 4 (~.053Å^{-1})*	*Best Matched Phase*
42	1	1	1.65	1.91	2.91	HCP
	2.5	1	1.68	1.97	2.96	HCP
	5	1	*DNE	1.98	2.91	Lamellar
	7.5	1	1.68	2.09	2.85	HCP
	10	1	1.66	1.97	2.96	HCP
	12.5	1	1.7	2.02	2.75	HCP
	15	1	1.65	1.96	2.93	HCP
60	1	1	1.7	1.99	2.94	HCP
	2.5	1	1.71	2.03	2.9	HCP
	5	1	*DNE	1.99	2.98	Lamellar
	7.5	1	1.68	1.97	2.81	HCP
	10	1	1.66	1.98	2.97	HCP
	12.5	1	1.68	1.99	2.84	HCP
	15	1	1.7	1.99	2.81	HCP
77	1	1	1.7	1.99	2.93	HCP
	2.5	1	1.66	1.97	2.7	HCP
	5	1	*DNE	1.98	2.99	Lamellar
	7.5	1	1.7	1.98	2.98	HCP
	10	1	1.64	1.97	3	HCP
	12.5	1	1.65	1.97	3.01	HCP
	15	1	1.69	2.08	2.86	HCP
Pure PS-PI-PS	0	1	1.7	1.98	2.78	HCP

*DNE - no peak was found in this range and no ratio can be calculated
**HCP – Hexagonally Packed Cylinders

Table S1: Peak ratios for all peaks for 42 kDa, 60 kDa, and 77 kDa RRe-P3HT blends with PS-PI-PS. Phases are assigned to best matched ratio, but there is some variability in ratios, so matching is not absolute or isolated to a single phase.

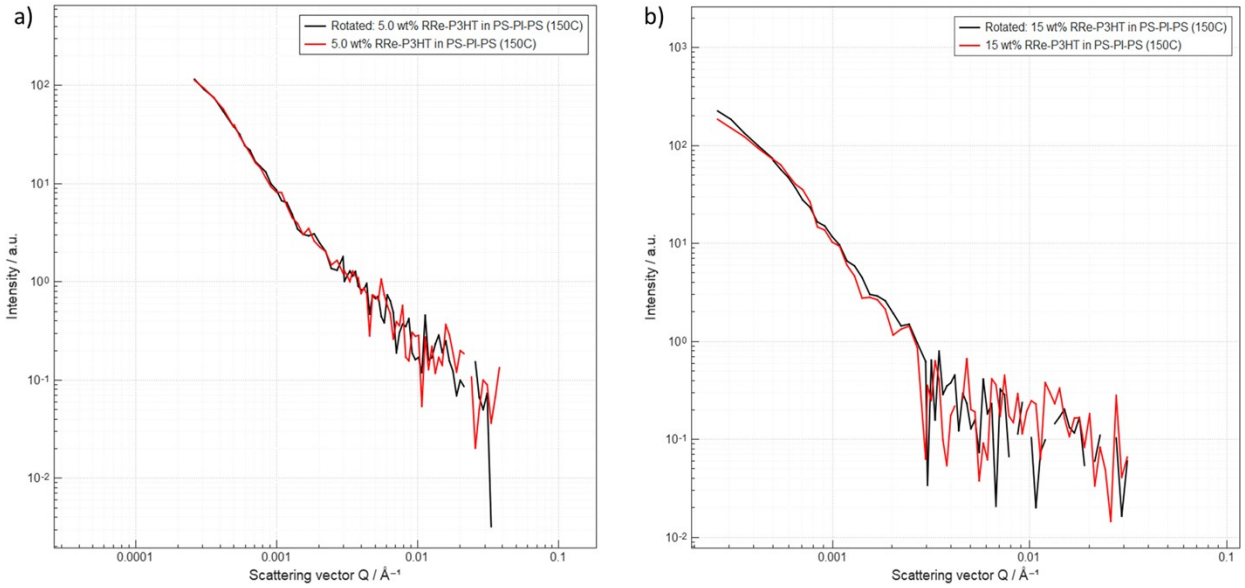

Figure S11: USAXS data for a) 5 wt% RRe-P3HT in PS-PI-PS pressed at 150 ºC and b) 15 wt% RRe-P3HT in PS-PI-PS pressed at 150 ºC, taken at two measurements, with one with the sample rotated 90º. The overlap show between the two samples suggests the feature is not an aligned or oriented sample and information is not lost in a line collimated Bonse-Hart measurement setup.

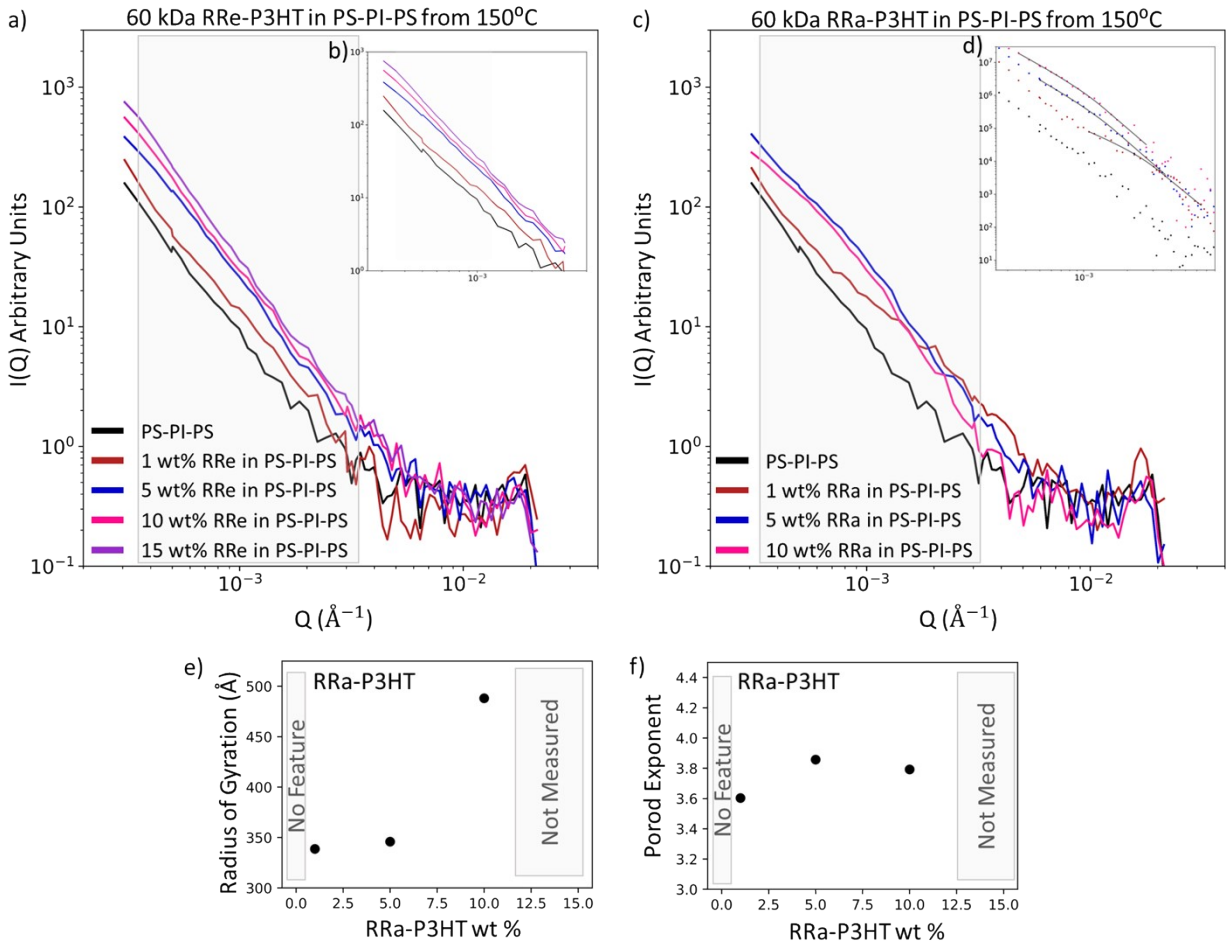

Figure S12 a) full smeared USAXS low-Q data of 60 kDa RRe-P3HT and PS-PI-PS blends processed at 150 ºC with region of interest marked in grey and peak analyzed in SAXS data visible in high-Q indicating data overlap. b) zoom of region of interest of low-Q region of smeared USAXS data of 60 kDa RRe-P3HT and PS-PI-PS blends processed at 150 ºC. c) full smeared USAXS low-Q data of 63 kDa RRa-P3HT and PS-PI-PS blends processed at 150 ºC with region of interest marked in grey and peak analyzed in SAXS data visible in high-Q indicating data overlap. d) zoom of region of interest of low-Q region of desmeared USAXS data of 63 kDa RRa-P3HT and PS-PI-PS blends processed at 150 ºC with Guinier-Porod fits. Data points are plotted as points and Guinier-Porod fits are plotted using black lines. Guinier-Porod fit parameters for 63 kDa RRa-P3HT were extracted and e) radius of gyration and f) Porod exponent is plotted against weight percent of conjugated polymer added.

At low (150 ºC) temperatures, with the addition of RRe-P3HT conjugated polymer we observe deviation from the power law slope of the PS-PI-PS background, but there is reduced clarity in the emergence of a feature. These features are not clear enough to be fit using a Guinier-Porod model, therefore no fits are shown in **Figure S12b** and no parameter plots shown. Clear features are formed with the addition of RRa-P3HT into the PS-PI-PS matrix. Features are formed earlier than with the RRe-P3HT, with a clear featuring forming in the 1 wt% RRa-P3HT sample and features still visible in the length scales observed for the 5 and 10 wt%. This suggests that large scale amorphous structures are formed with the addition of any RRa-P3HT conjugated polymer, and the size of the structures are generally smaller than their semi-crystalline counterparts. We see at low conjugated polymer loadings (i.e. weight percent) the extracted radius of gyration of these features is smaller than the 250 ºC RRe-P3HT analog, but at 10 wt% the size increases drastically. This feature is larger than that found in any of the samples formed in the 250 ºC RRe-P3HT blends. We also see that the interface between the large scale RRa-P3HT amorphous structures and the surrounding PS-PI-PS is not completely smooth, as can be observed with Porod exponents in the range of 3.6-3.8. The smoothness of this interface increases as the weight percent of RRa-P3HT increases but it does not reach the limits of a completely smooth and sharp interface, which would result in a Porod exponent of 4.0.

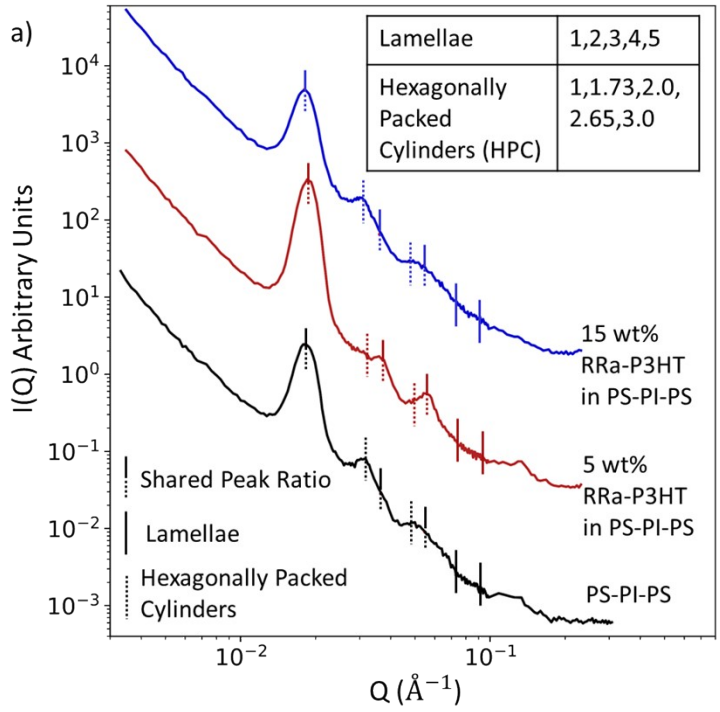

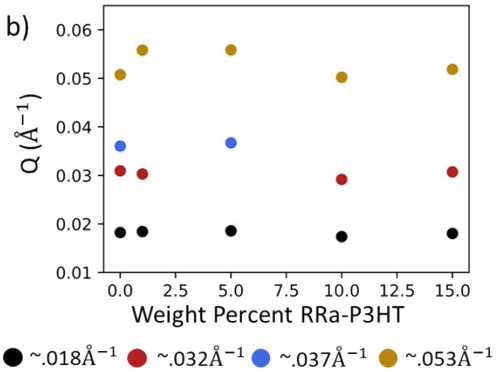

c)

Sample	Peak Ratios ($\frac{Q_{peak\ i}}{Q_{peak\ 1}}$)				Phase
Wt% RRa-P3HT	*Peak 1 (~.018 Å^{-1})*	*Peak 2 (~.032 Å^{-1})*	*Peak 3 (~.037 Å^{-1})*	*Peak 4 (~.053 Å^{-1})*	*Best Phase*
0	1	1.7	2.08	2.78	HCP
1	1	1.64	*DNE	3.03	HCP
5	1	*DNE	1.98	3.01	Lamellae
10	1	1.70	*DNE	2.89	HCP
15	1	1.70	*DNE	2.88	HCP

Figure S13: a) SAXS data of selected 63 kDA RRa-P3HT and PS-PI-PS blends, labeled by wt% of RRa-P3HT added to system, and collected at 250 ºC. Data is arbitrarily shifted to separate samples into wt%. Lines are added to mark where peaks are expected for lamellar and hexagonally packed cylinder structures. Some locations overlap between the two and are noted with solid lines.b) peak position parameters from broad peak fits of all peaks with colors dictated by legend above. c) peak ratios for all samples, with best assigned phase named.

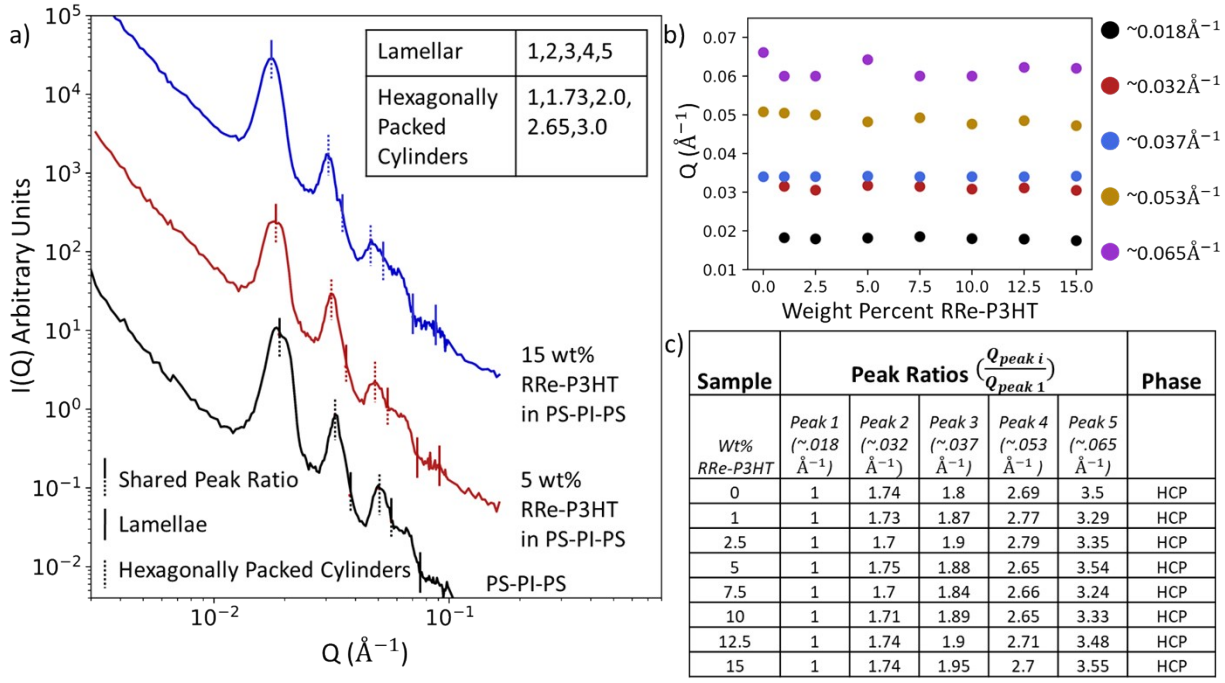

c)

Sample	Peak Ratios ($\frac{Q_{peak\ i}}{Q_{peak\ 1}}$)					Phase
Wt% RRe-P3HT	*Peak 1 (~.018 Å^{-1})*	*Peak 2 (~.032 Å^{-1})*	*Peak 3 (~.037 Å^{-1})*	*Peak 4 (~.053 Å^{-1})*	*Peak 5 (~.065 Å^{-1})*	
0	1	1.74	1.8	2.69	3.5	HCP
1	1	1.73	1.87	2.77	3.29	HCP
2.5	1	1.7	1.9	2.79	3.35	HCP
5	1	1.75	1.88	2.65	3.54	HCP
7.5	1	1.7	1.84	2.66	3.24	HCP
10	1	1.71	1.89	2.65	3.33	HCP
12.5	1	1.74	1.9	2.71	3.48	HCP
15	1	1.74	1.95	2.7	3.55	HCP

Figure S14: a) SAXS data of selected intentionally aligned 60 kDA RRe-P3HT and PS-PI-PS blends, labeled by wt% of RRe-P3HT added to system, and collected at 250 ºC. Data is arbitrarily shifted to separate samples into wt%. Lines are added to mark where peaks are expected for lamellar and hexagonally packed cylinder structures. Some locations overlap between the two and are noted with solid lines. b) peak position parameters from broad peak fits of all peaks with colors dictated by legend above. c) peak ratios for all samples, with best assigned phase named.

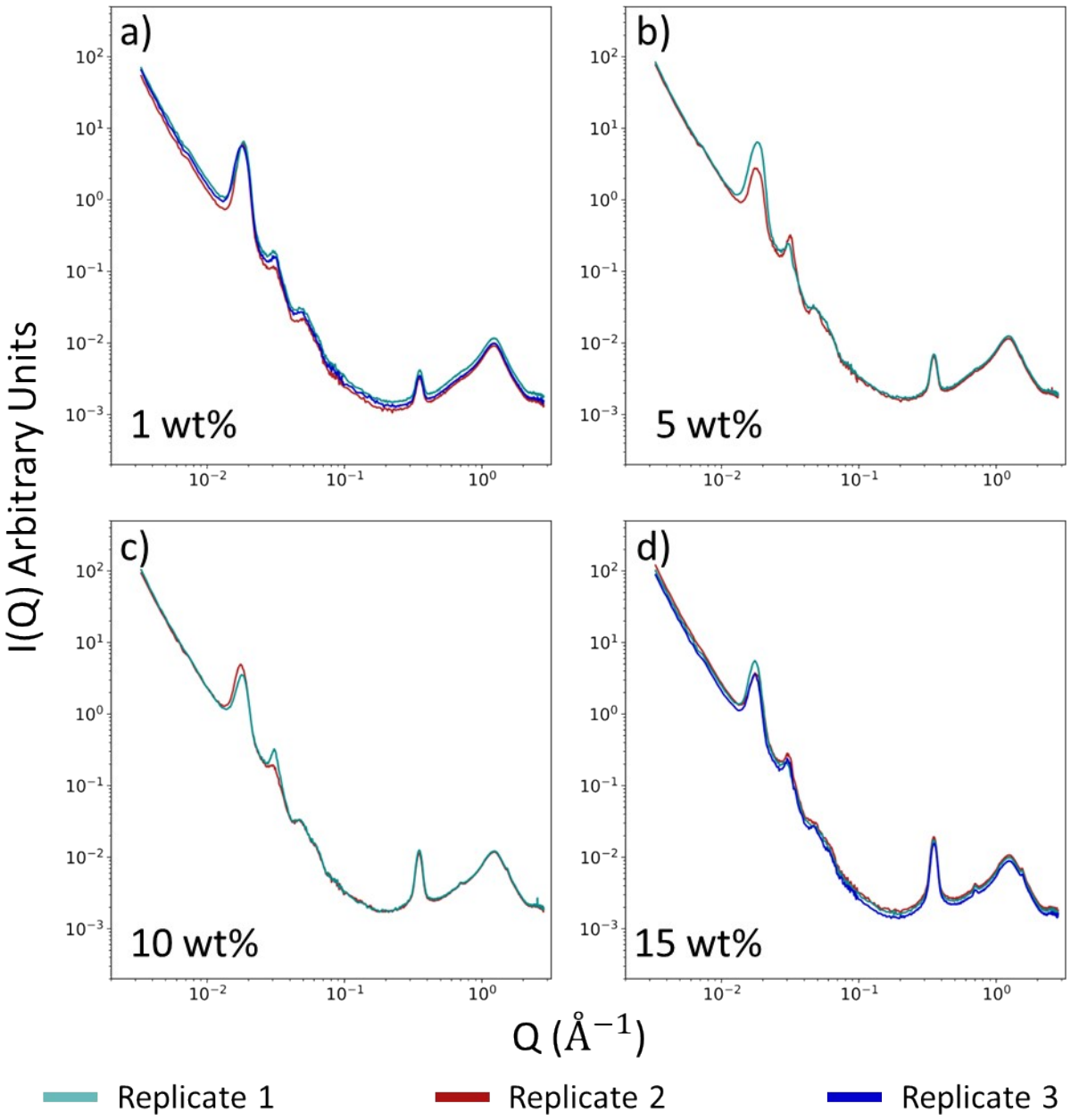

Figure S15: SAXS data of repeated intentionally aligned 60 kDA RRe-P3HT and PS-PI-PS blends, labeled by wt% of RRe-P3HT added to system, and collected at 250 ºC. Repeated samples agree at low and high weight percents, with more variability in the consistency of flow in the 5-10 wt% range.

Degree of Orientation

$$\Delta S = \lambda_1 - \lambda_2 = \sqrt{(S_{11} - S_{22})^2 + 4{S_{12}}^2} \quad \text{(S1)}$$

For an isotropic sample then $\lambda_1 = \lambda_2$, i.e. the similarity transforms lead to the identity matrix. This definition holds true for two-fold symmetry but would need to be updated for higher fold symmetries.

Anisotropy tensor

$$S = \begin{pmatrix} S_{11} & S_{12} \\ S_{21} & S_{22} \end{pmatrix} \quad \text{(S2)}$$

Elements of tensor

$$S_{11} = \langle \cos^2 \Psi \rangle = \frac{\int_0^{2\pi} d\Psi I(\Psi) \cdot \cos^2 \Psi}{\int_0^{2\pi} d\Psi I(\Psi)} \quad \text{(S3)}$$

$$S_{22} = \langle \sin^2 \Psi \rangle = \frac{\int_0^{2\pi} d\Psi I(\Psi) \cdot \sin^2 \Psi}{\int_0^{2\pi} d\Psi I(\Psi)} \quad \text{(S4)}$$

$$S_{12} = S_{21} = \langle \sin \Psi \cos \Psi \rangle = \frac{\int_0^{2\pi} d\Psi I(\Psi) \cdot \sin \Psi \cos \Psi}{\int_0^{2\pi} d\Psi I(\Psi)} \quad \text{(S5)}$$

Where Ψ is the azimuthal angle in the imagery convention (values increase anti-clockwise the reference for zero is the X axis at 3 o'clock.

Flexible Cylinder Model

This model is a shape dependent model that describes a flexible cylinder as described below.

$$S_{SB}(q,L,b) = S_{exv}(q,L,b) + C(\frac{L}{b})\left[\frac{4}{15} + \frac{7}{15u} - \left(\frac{11}{15} + \frac{7}{15u}\right)e^{-u}\right]\frac{b}{L} \quad \text{(S5)}$$

where L is length of the cylinder, b is Kuhn length, and

$$u = \langle {R_g}^2 \rangle_0 q^2 \quad \text{(S6)}$$

$$S_{exv}(q,L,b) = w(qR_g)S_{Debye}(q,L,b) + [1 - w(qR_g)][C_1(\quad \text{(S7)}$$

where $\langle {R_g}^2 \rangle_0$ is the ensemble average of the square of the radius of gyration and

$$w(qR_g) = [1 + \tanh((qR_g - C_4)/C_5)]/2 \quad \text{(S8)}$$

$$S_{Debye}(q,L,b) = \frac{2[e^{-u} + u - 1]}{u^2} \quad \text{(S9)}$$

Further individual parameter values and system dependent definitions are provided in the original derivation.

Source for the equations and derivation is: Pedersen, J. S. & Schurtenberger, P. Scattering functions of semiflexible polymers with and without excluded volume effects. *Macromolecules* **29**, 7602–7612 (1996)